**Author for correspondence:**

M.G. Worster

e-mail: mgw1@cam.ac.uk

# Sea ice thermodynamics and brine drainage

M. Grae Worster[1] and David W. Rees Jones[2]

[1]Institute of Theoretical Geophysics, DAMTP, CMS Wilberforce Road, Cambridge CB3 0WA UK
[2]Atmospheric, Oceanic and Planetary Physics, Department of Physics, University of Oxford, Oxford, UK

Significant changes in the state of the Arctic ice cover are occurring. As the summertime extent of sea ice diminishes, the Arctic is increasingly characterised by first-year rather than multi-year ice. It is during the early stages of ice growth that most brine is injected into the oceans, contributing to the buoyancy flux that mediates the thermo-haline circulation. Current operational sea-ice components of climate models often treat brine rejection between sea ice and the ocean similarly to a thermodynamic segregation process, assigning a fixed salinity to the sea ice, typical of multi-year ice. However, brine rejection is a dynamical, buoyancy-driven process and the salinity of sea ice varies significantly during the first growth season. As a result, current operational models may over predict the early brine fluxes from newly-formed sea ice, which may have consequences for coupled simulations of the polar oceans. Improvements both in computational power and our understanding of the processes involved have led to the emergence of a new class of sea-ice models that treat brine rejection dynamically and should enhance predictions of the buoyancy forcing of the oceans.

In this article, we review some fundamentals of the thermodynamic growth of sea ice (section 1) and illustrate the different magnitudes of buoyancy flux resulting from cooling and brine rejection in polynyas and from consolidated sea ice (section 2). We review in section 3 some of the fundamental principles governing convection in sea ice, emphasising the key role of the Rayleigh number in determining the existence and strength of brine drainage. We describe experimental observations of the formation of brine channels and their consequences (section 4), highlighting in particular the way in which the salinity and porosity of sea ice decrease as a result of the upwards flow of ocean water that compensates for the downwards flow through brine channels. We culminate in section 5 by describing and comparing recent one-dimensional models of brine drainage parameterised by local Rayleigh numbers, which allow profiles of sea-ice salinity to be computed dynamically and can be incorporated at reasonable computational cost into ice components of climate models.

## 1. Thermodynamic growth of sea ice

Sea ice is a mushy layer [1] comprising a porous matrix of essentially pure ice crystals filled with brine. The (bulk) salinity of sea ice $S$ is related to the salinity of the interstitial brine $S_{br}$ by

$$S = (1 - \phi)S_{br}, \tag{1.1}$$

where $\phi(\mathbf{x}, t)$ is the local volume fraction occupied by ice crystals.

The simplest model of sea-ice growth assumes a quasi-steady (linear) temperature across a layer of constant and uniform solid fraction and computes its thickness $h(t)$ from the Stefan condition

$$\rho_s L \phi \frac{dh}{dt} = k \frac{T_f - T_s}{h}, \tag{1.2}$$

where $\rho_s$ is the density of pure ice, $L$ is the latent heat of fusion per unit mass, $k(\phi)$ is the thermal conductivity of sea ice, $T_f$ is the freezing temperature of the ocean, $T_s$ is the surface temperature of the sea ice in contact with the atmosphere and $t$ is time. For constant temperatures at the boundaries, equation 1.2 is readily integrated to give

$$h(t) = \sqrt{2 \frac{k(\phi)}{\phi} \frac{T_f - T_s}{\rho_s L} t}. \tag{1.3}$$

It appears therefore that thermodynamic growth of sea ice depends on its solid fraction, which depends on its salinity. However, to a good approximation, given that the ice platelets in sea ice are oriented vertically (their c-axes are dominantly horizontal), the conductivity of sea ice can be estimated by

$$k(\phi) = \phi k_s + (1 - \phi)k_{br}, \tag{1.4}$$

where $k_s$ and $k_{br}$ are the conductivities of pure ice and of brine respectively. Therefore

$$\frac{k(\phi)}{\phi} = k_s \left( 1 + \frac{1 - \phi}{\phi} \frac{k_{br}}{k_s} \right) \approx k_s, \tag{1.5}$$

which is approximately independent of $\phi$ both because $k_s$ is about five times larger than $k_{br}$ and because $\phi$ tends to be a rather large fraction through most of the sea ice. Physically, one sees from equation 1.3 that there are partially compensating influences of enhanced thermal conductivity competing with increased release of latent heat when the solid fraction is larger. Such compensation also occurs in more detailed models of mushy layers in which the solid fraction varies in time and space.

This very simple illustration shows that if one is simply interested in the thickness of sea ice then an accurate estimation of salinity or brine volume may not be critical. What this model (essentially a zero-layer Semtner model [2], which proposes simplifications of the detailed model of Maykut & Untersteiner [3]) lacks is any account of the heat capacity of sea ice; within the model,

the growth and heat transfers between ocean, ice and atmosphere respond instantaneously to changes in forcing. The model is therefore not generally good at responding with the appropriate phase lag to variations in forcing, whether diurnal, synoptic or seasonal.

The effective heat capacity of sea ice is affected significantly by internal release of latent heat as the solid fraction varies in time. This is seen most readily from the thermal energy equation (in the absence of fluid flow)

$$\overline{\rho c_p} \frac{\partial T}{\partial t} = \nabla \cdot (k \nabla T) + \rho_s L \frac{\partial \phi}{\partial t}, \tag{1.6}$$

in which the role of latent heat as an internal heat source as the solid fraction varies is transparent. The left-hand side of equation 1.6 is the rate of change of enthalpy with time, noting that the specific heat capacity is equal to the derivative of enthalpy with respect to temperature at constant pressure [4]. The mean sensible heat capacity per unit volume is

$$\overline{\rho c_p} = \phi \rho_s c_s + (1 - \phi) \rho_{br} c_{br}, \tag{1.7}$$

where $c_s$ and $c_{br}$ are the specific heat capacities of pure ice and of brine respectively, and $\rho_{br}$ is the density of brine. From equation 1.1, relating the solid fraction and the interstitial concentration, and a statement of the freezing-point depression of water caused by salt (the liquidus equation)

$$T = T_m - m S_{br}, \tag{1.8}$$

in which $T_m = 0^\circ$C is the freezing temperature of pure water and $m \approx 0.05^\circ$C ppt$^{-1}$ is the liquidus slope, we can determine that the temperature satisfies a nonlinear diffusion equation

$$c \frac{\partial T}{\partial t} = \nabla \cdot (k \nabla T), \tag{1.9}$$

in which the effective heat capacity

$$c(S, T) = \overline{\rho c_p} + \rho_s L \frac{mS}{(T_m - T)^2}. \tag{1.10}$$

Note that an assumption is made that the interior of a mushy layer is in local thermodynamic equilibrium so that the liquidus relationship 1.8 holds throughout the layer [1].

The effective heat capacity is dominated by the term involving the latent heat, which is dependent also on the salinity of the sea ice. In deriving equation 1.9 it has been assumed that the bulk salinity is quasi-steady so that $\partial S / \partial t \approx 0$. The one-layer Semtner model of sea-ice growth [2] is essentially a discretised implementation of this diffusion equation with a single grid point at mid depth in the sea ice. Similarly, CICE version 4 [5] (for example) implements the diffusion equation 1.9 on a small number (often 4) of discrete layers, which could be increased if felt necessary as computing power increases. In both cases, the salinity of the sea ice is prescribed, either as a constant or as a given profile.

These sorts of approaches improve the thermodynamic description of sea-ice evolution but there are important questions to be addressed. The typical estimations of ice salinity of about 4 ppt used to determine the effective heat capacity are more typical of relatively thick, late-season or multi-year ice, from which the brine flux is relatively small, than of the early formations of ice in leads, from which the brine flux is more significant. They are also based on observations of ice formed in median ocean salinities (around 35 ppt) and may be less appropriate for scenarios involving a freshening ocean or currently in regions of brackish water such as the Baltic Sea. Ideally, a model of the thermodynamic growth and evolution of sea ice should be robust to changing climate scenarios and of utility regardless of regional variations of ocean salinity. To this end there have been recent efforts to develop models in which the ice salinity profile is predicted dynamically, which is the focus of this article.

An additional reason for wanting to know or be able to predict changing ice salinity is to determine the buoyancy flux to the ocean, which is dominated in polar regions by brine fluxes associated with ice formation. Some current sea-ice models dissociate the processes of thermodynamic growth and brine rejection, sometimes specifying different ice salinities to

determine thermodynamic properties from those used to determine brine fluxes but ideally an internally consistent model should couple these elements.

The convective transport within sea ice plays a broader role within the climate system [6]. For example, convection supplies nutrients to the diverse microbiological community within sea ice and interact with the transport of trace gases through sea ice. There are potential physical feedbacks associated with biogeochemical transport, such as through ice albedo and atmospheric chemistry.

Before describing some new modelling approaches that provide an internal description of brine drainage, we first provide a more general discussion of buoyancy fluxes.

## 2. Buoyancy fluxes

The brine fluxes from growing sea ice make a significant contribution to the buoyancy forcing of the ocean. Considering an annual cycle, it is interesting to contrast the buoyancy flux resulting from cooling the surface waters prior to any ice formation with the buoyancy flux that results once ice begins to form either in an open polynya or in a region of consolidated ice.

Although sea water with salinity above about 24 ppt has a monotonic variation of density with temperature above its freezing temperature, the same physics that gives rise to the density maximum of pure water at 4°C gives polar sea water a strongly nonlinear equation of state with a thermal expansion coefficient $\alpha \approx 10^{-5}$ °C$^{-1}$ at its freezing temperature of around $-2$°C, compared with a value of $\alpha \approx 10^{-4}$ °C$^{-1}$ at 20°C. These values and the following estimates of buoyancy fluxes are only intended to illustrate orders of magnitude. Exact values depend on salinity as well as temperature.

The buoyancy flux to the ocean associated with cooling ice-free surface waters in the absence of newly-forming sea ice is

$$F_{BT} = \frac{g\alpha F}{c_p}, \tag{2.1}$$

where $g$ is the acceleration due to gravity and, here, $c_p$ is the specific heat capacity of the ocean. This buoyancy flux has a value of about 10 $\mu$W m$^{-3}$ when the surface heat flux from ocean to atmosphere $F \approx 400$ W m$^{-2}$ and the ocean is near to its freezing temperature. In contrast, within a polynya, where growing ice crystals are blown downwind and the open ocean is continuously exposed to the cold atmosphere, the buoyancy flux associated with the resulting brine flux is

$$F_{BS} = \rho_o g \beta S_o \frac{F}{\rho_s L}, \tag{2.2}$$

where $\beta$ is the fractional change in density associated with a change in salinity, and $\rho_o$ and $S_o$ are the density and salinity of the ocean. This brine-driven buoyancy flux has a value of about 300 $\mu$W m$^{-3}$ for the same heat flux. These typical buoyancy fluxes are illustrated in figure 1.

Once the ice consolidates and forms a columnar structure, it insulates the ocean from the cold atmosphere and the ice-ocean interface has a temperature very close to the freezing temperature of the ocean. The thermal buoyancy flux is then associated with the ocean heat flux, and if the ocean heat flux is about 6 W m$^{-2}$, for example, then the associated buoyancy flux is only about 0.2 $\mu$W m$^{-3}$. On the other hand, brine continues to drain from the columnar sea ice, and leads to a time-varying buoyancy flux, illustrated in figure 1. The figure also illustrates the different prediction of buoyancy flux made if the salinity of the ice is assumed to be fixed at 4 ppt rather than evolving dynamically, as described in section 5 below. For now, we simply note that the prediction made using a dynamically-evolving salinity reaches a maximum value within the first day or so that is about a fifth of that from an open polynya.
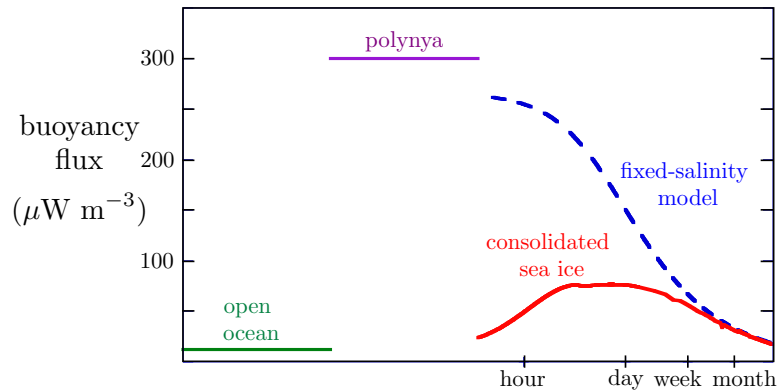
**Figure 1.** The buoyancy fluxes resulting from cooling in an open ocean, brine release in an open polynya or from consolidated sea ice. In the first two cases the heat flux to the atmosphere is fixed at 400 W m$^{-2}$, while in the third case the atmospheric temperature and the heat transfer coefficient between the ice surface and the atmosphere are held fixed such that the heat flux is 400 W m$^{-2}$ when the temperature difference is $20^\circ$C. The buoyancy fluxes in the open ocean and polynya are constant and the figure simply indicates their value; the logarithmic time axis relates only to the consolidated sea ice. The blue dashed curve shows the buoyancy flux predicted if the sea ice is assumed to have a fixed salinity $S = 4$ ppt.

# 3. Fundamentals of convection in sea ice

The brine in the interstices of sea ice is much saltier and therefore denser than the sea water from which the sea ice formed. It therefore has potential energy that can be released by brine draining from the sea ice into the ocean. It is well known that fluid systems that are statically unstable, having a density that increases with height, can be dynamically stable if their Rayleigh number is insufficiently large. The Rayleigh number characterises the potential energy available to drive fluid motion relative to the dissipation of that energy both by viscosity and by diffusion of the agent causing the density variations. A parcel of interstitial fluid of size $d$ in sea ice has potential energy

$$PE \sim [\rho_{br}(z) - \rho_o]d^3 g(h - z) \tag{3.1}$$

relative to the ocean, where $z$ is the vertical position of the fluid parcel measured downwards from the surface of the ice.

In the net movement of the parcel downwards and the compensating flow upwards through the porous mushy layer there is dissipation of energy

$$D \sim \Delta p \, d^2 (h - z) \sim \frac{\mu U}{\Pi}(h - z)d^2(h - z) \sim \frac{\mu}{\Pi}\frac{d^2(h - z)^3}{\tau}, \tag{3.2}$$

where $U$ characterises the magnitude of the fluid motion (Darcy velocity) and $\tau \sim (h - z)/U$ characterises the time over which the the exchange of potential energy takes place. The other variables are the pressure difference $\Delta p$ between the location of the parcel and the ocean; the dynamic viscosity of brine $\mu$; and the permeability of the porous sea ice $\Pi$.

The motion can only be sustained if the dissipation is less than the potential energy available, which argues for slow motion releasing the potential energy over a long time. On the other hand, if the movement takes too long then the buoyancy will be dissipated by a combination of diffusion and phase change as follows.

The parcel, which is assumed to be much larger than the pore scale, tends to equilibrate its temperature with its new surroundings on a time scale mediated by thermal diffusion. Because the diffusivity of salt is very much less than that of heat, the parcel will not decrease in salinity as

quickly by diffusion but will instead dissolve some ice until its salinity matches the liquidus value corresponding to its temperature. Thus the parcel loses its buoyancy on a time scale determined by thermal diffusion. In order to release this potential energy as kinetic energy of convection, $\tau$ should not be long compared with the thermal diffusion time $d^2/\kappa$.

Bearing in mind the dual constraints of viscous and diffusive dissipation of the potential energy, it is optimal if $\tau \sim d^2/\kappa$ and there will be convection if $PE \gtrsim D$, so if

$$[\rho(z) - \rho_o]d^3 g(h-z) \gtrsim \frac{\mu}{\Pi} \frac{(h-z)^3}{\kappa}. \tag{3.3}$$

From this expression, we see that larger scale motions (large $d$) are preferred and that the optimal energy transfer is achieved when the fluid motions span the full depth of the domain so that $d \sim h - z$ and the Rayleigh number

$$R_m(z) \equiv \frac{g'(z)(h-z)\Pi(z)}{\kappa \nu} > \mathrm{O}(1), \tag{3.4}$$

where $g'(z) = [\rho(z) - \rho_o]g/\rho_o$ is a reduced gravity and $\nu = \mu/\rho_o$ is the kinematic viscosity of the brine.

Note that these fundamental physical principles and the associated scaling analysis apply also to convection in a mushy layer once brine channels have formed, as described below . The downflow is then principally through the channels but must be compensated by upflow through the surrounding mushy layer, which provides the dominant resistance to the convective flow of the system.

Theoretical studies of idealised settings [7] have shown that a motionless state is unstable and convection is predicted in a mushy layer that is open to a fluid region when the Rayleigh number exceeds a critical value of about 10. This is comparable to the critical Rayleigh number below which convection with liquid channels shuts down [8]. Note that the thermal diffusivity $\kappa$ in this estimation should be taken to be $k/c$, taking account of the enhanced specific heat capacity resulting from latent heat release and the phase-averaged thermal conductivity. Often, using simple, dimensional scaling, a Rayleigh number $R_m^*$ is initially defined in terms of the thermal diffusivity of the liquid phase [9] [10]; however, it can then be shown [7] that it is the parameter grouping $R_m = \Omega R_m^*$ that must exceed a critical value for convection to ensue, where $\Omega$ is the factor by which the specific heat capacity is augmented by latent heat release.

Flow through mushy layers causes dissolution of the solid phase when directed from cooler to warmer regions [11]. Thus downflow in sea ice during growth has a tendency to form brine channels, which form the principal conduit for brine drainage into the ocean, as described below. Conversely, upflow through the mushy region outside the channels promotes further solidification, which can lead to the confinement of convection near the ice–ocean interface, as described and predicted in section 5 below.

## 4. Experimental observations of brine fluxes from sea ice

Laboratory experiments in which salt water is cooled and solidified from above show clearly the formation and structure of mushy layers of ice, with a porous matrix of dominantly vertical ice platelets punctured by brine channels (figure 2). A study of ice mushy layers using Magnetic Resonance Imaging [12] has revealed the evolution of brine channels and shown that freshening of the layers is associated with the presence of channels. Dense brine emerges from brine channels to form strong plumes injecting salt into the underlying liquid, punching through any putative laminar sublayer in a turbulent parameterisation of brine fluxes at the ice–ocean interface. Brine fluxes are rather determined by convection internal to sea ice; a laminar flow down brine channels supplied by upflow from the ocean through the surrounding mushy layer.

Experiments in which the rate of solidification was controlled and steadily growing states were achieved [13] have confirmed that brine channels form once the Rayleigh number is large enough and that convection ceases if the Rayleigh number subsequently decreases sufficiently, while
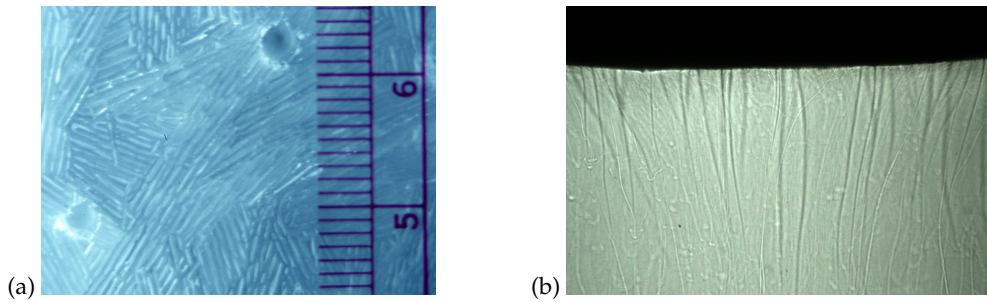
**Figure 2.** (a) The underside of sea ice grown in the laboratory [10] showing the ends of ice platelets with a micro scale of a little less than 1 mm punctured by brine channels with a diameter of about 3 mm. (b) Side view shadowgraph showing plumes of dense brine emanating from brine channels in sea ice grown in the laboratory after about 6 hours of growth (photograph by S. Peppin). The width of the view is about 20 cm.

growth continues. The fundamental idea that brine drainage is not directly linked to growth was also demonstrated [10] in experiments in which significant brine drainage only began once the layer of sea ice was sufficiently thick and therefore its associated Rayleigh number was sufficiently large.

A key experimental observation [12] is that brine channels need not occupy the full depth of the mushy layer and that brine drainage is confined to that part of the mushy layer that contains (active) brine channels (see figure 3). The interpretation is that in those cases the local Rayleigh number, as defined by equation 3.4, exceeds the critical value only in a region of the mushy layer adjacent to the mush–liquid interface. This idea was also explored in interpretations of field measurements of sea ice [14], where it was found that the local Rayleigh number peaked a few centimetres above the ice–ocean interface and had very small values higher in the layer of sea ice. The peak value of the Rayleigh number was also found to hover around a fairly constant value, much lower than the value that would have been attained had brine drainage and freshening of the sea ice not occurred.

Equation 3.4 shows that the Rayleigh number increases with height above the ice–ocean interface as the potential energy driving convection, proportional to $[\rho(z) - \rho_o](h - z)$, increases but decreases as the permeability $\Pi(z)$ decreases either in response to colder temperatures or to lower bulk salinities. For example, the permeability can be estimated as $\Pi = \Pi_0(1 - \phi)^3 = \Pi_0(S/S_{br})^3$, as used by [10] and which approximates the expression suggested by Freitag [15]. Then if the bulk salinity $S$ is uniform, $\Pi = \Pi_0(S/S_{br})^3$ and

$$R_m = \frac{\beta \left[S_{br}(z) - S_o\right] g(h - z)\Pi_0(S/S_{br})^3}{\kappa\nu} = \frac{\beta g \Pi_0 m^2 S^3}{\kappa\nu} \frac{T_f - T_s}{[T_m - T(z)]^3} \frac{(h - z)^2}{h} \tag{4.1}$$

when the temperature field

$$T(z) = T_f - (T_f - T_s)\frac{h - z}{h} \tag{4.2}$$

is linear, and we get the profile shown in figure 5(a) below. Once convection begins, brine drains through the brine channels to the ocean and the necessary return flow brings relatively fresh water upwards from the ocean into the sea ice where it partially freezes to increase the solid fraction and reduce the permeability. Thus convection in a mushy layer is self-regulating.

The fundamental ideas and observations of the preceding two sections have recently been brought together into new, one-dimensional parameterisations of brine drainage in sea ice.
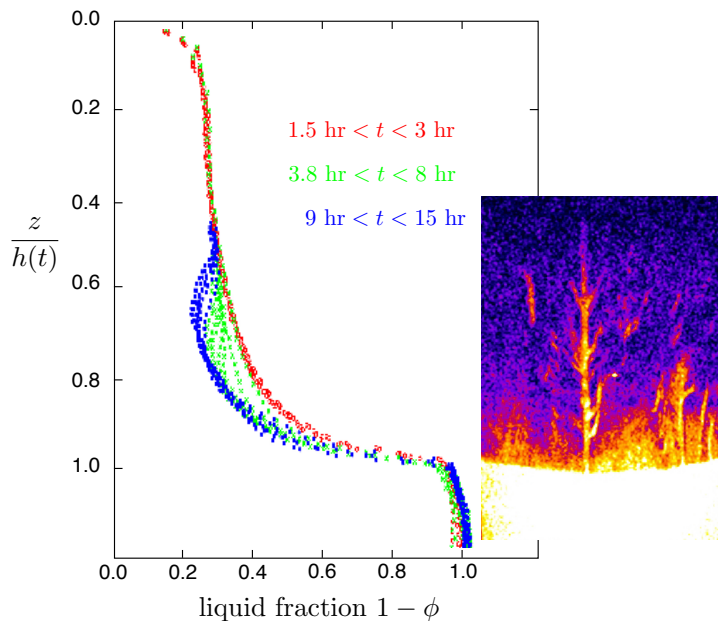
**Figure 3.** MRI (Magnetic Resonance Imaging) measurements of liquid fraction $1 - \phi$ in an ice mushy layer grown from a sugar solution as it evolves in time [12]. For the first few hours there are no brine channels and the liquid fraction has a self-similar profile. Once channels form, the liquid fraction decreases (the solid fraction increases). The inset shows an MRI of the lower portion of the mushy layer aligned with the measurements. The reduction in concentration and liquid fraction is associated with the region in which channels exist.

## 5. Theoretical modelling of brine drainage

Detailed, albeit idealised, two-dimensional, numerical calculations of flow in a mushy layer with brine channels have been made by Chung & Worster [8] and by Wells *et al.* [16]. Both studies analysed a periodic array of channels and determined the brine flux from a single channel as it varies with Rayleigh number. But whereas Chung & Worster left open the question of what determines the spacing between channels and, therefore, the total brine flux, Wells *et al.* introduced the hypothesis that the channel spacing optimises the total flux. Not only did they show with their numerics that such an optimal flux is achieved at a finite, non-zero and sensible spacing, similar to that seen experimentally, they showed that the optimal flux correlates well in a linear relationship with the Rayleigh number [17].

Such calculations are computationally expensive, and a step towards a simpler, mostly analytical model of brine drainage, the so-called Chimney-Active-Passive (CAP) model, was developed by Rees Jones & Worster [18], see figure 4. Within the approximations of the CAP model, including an assumption of large supercritical Rayleigh numbers, they showed analytically that the net brine flux in two dimensions is linearly related to the Rayleigh number. They extended their model to three dimensions, where they found that the linear relationship was maintained approximately. The CAP model also showed (in the idealised setting) that the vertical component of velocity through most of the mushy layer decreased linearly with height above the ocean to zero at the top of the convecting region.

Three models of brine drainage from sea ice have emerged in the last year or so that are based on conceptions of buoyancy-driven flow through brine channels and have the potential to be computationally cheap enough to be incorporated into climate models [19], [20], [21]. Indeed, the
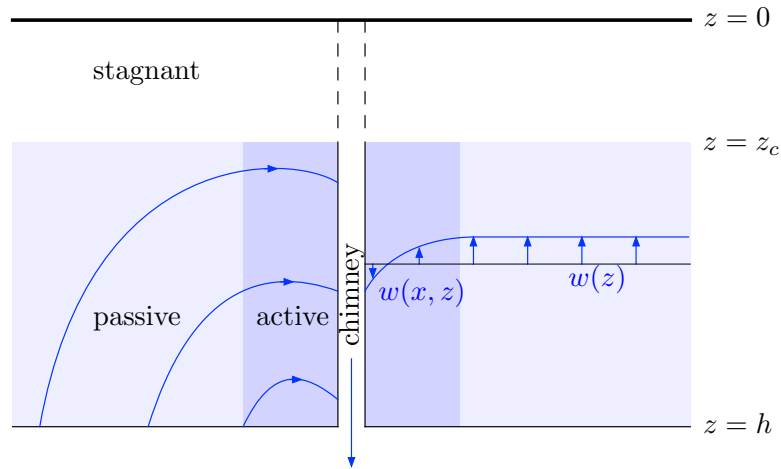
**Figure 4.** The CAP model [18] showing a vertical chimney (brine channel) surrounded by an active region in which buoyancy provides a baroclinic torque to turn the flow fed from a passive region in which the flow is driven primarily by pressure gradients rather than buoyancy. The left-hand side shows streamlines, while the right-hand side shows the vertical velocity component, which is horizontally uniform in the passive region. The top of the convecting region is denoted by $z_c$, above which $z < z_c$ and the sea ice is stagnant.

model of Turner *et al.* [19] is now included as an option within CICE version 5 [22]. They share the common assumption, based on the observations above of more detailed models, that the brine flux varies linearly with the Rayleigh number. They each begin by computing the local value of the Rayleigh number $R_m(z)$ defined by equation 3.4. There are minor differences according to whether the permeability is taken to be the minimum value or the harmonic mean of $\Pi(z)$ between $z$ and the ice-ocean interface. The latter is more appropriate in the calculation of the pressure difference in 3.2 but the two estimations not too different given that the harmonic mean value is dominated by the lower values. An example profile of $R_m(z)$ is shown in figure 5(a). If the Rayleigh number exceeds a critical value $R_c$ anywhere in the domain then it is assumed that there is a horizontally uniform upwards flow $w(z)$ providing the return flow for brine draining downwards through brine channels. The continuum profiles of the return flow implied by the three models differ slightly as follows.

Turner *et al.* [19] take the flow rate to be the largest of the flow rates they calculate for layers at or above the layer in question. The dominant character of this choice is illustrated by the expression

$$w(z) = -\max_{\zeta < z}[\alpha(\zeta)(R_m(\zeta) - R_c)], \tag{5.1}$$

where $\alpha(z)$ is a positive function, bounded away from zero, that measures some of the internal dimensions of the mushy layer as well as its material properties.

Griewank & Notz [20] calculate a local downflow at each level, proportional to the amount by which the local Rayleigh number exceeds a critical value, and sum these for all levels above the level in question to determine the upflow there. This is illustrated by the expression

$$w(z) = -\alpha \int_0^z [R_m(\zeta) - R_c] \, d\zeta. \tag{5.2}$$

Based on their CAP model, Rees Jones & Worster [21] assume a simple linear velocity profile across the convecting region, with its magnitude determined by the maximum value of the Rayleigh number, so that

$$w(z) = -\alpha \max_{\zeta}[R_m(\zeta) - R_c] \, (z - z_c), \tag{5.3}$$

where $z_c$ is the minimum value of $z$ for which $R_m(z) \geq R_c$.

In each of these expressions, which are illustrated in figure 5, the term in square brackets is taken to be zero if the value inside the brackets is negative, i.e. if $R_m(z) < R_c$. In many scenarios, such as that shown in figure 5, the three expressions lead to broadly similar velocity profiles, in that all are monotonic and confined to a region of the sea ice close to the ice–ocean interface, and all provide for convection to cease once the Rayleigh number is too small. Turner *et al.* estimate the magnitude of convection $\alpha$ by equating the dynamic pressure drop along the channel with that driving a vertical return flow through the surrounding mush. Rees Jones & Worster calculate $\alpha$ in the idealised setting explored with their CAP model [18] but suggest that in the context of sea ice it is best treated as a tuning parameter [21], as is also done by Griewank & Notz [20]. Although various stability analyses have determined critical Rayleigh numbers in different settings, all three sets of authors treat the constant $R_c$ as a tuning parameter, which seems appropriate for use in the complex settings of real sea ice.
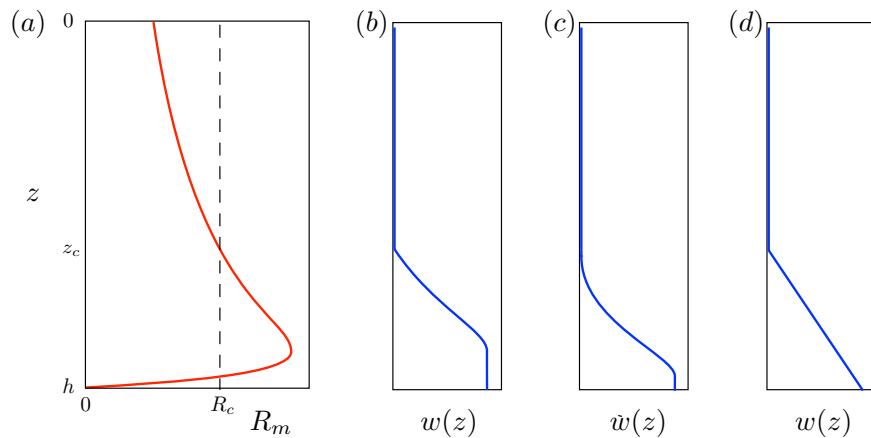


**Figure 5.** (a) An example of the Rayleigh number profile when the salinity is uniform and the temperature field is linear. The corresponding vertical velocity profiles are shown as modelled by (b) Turner *et al.* [19], (c) Griewank & Notz [20] and (d) Rees Jones & Worster [21]. Note that the velocities are shown without scale because each model tunes the amplitude of the velocity profile.

With the vertical velocity computed as above, the ice salinity is updated using the local salt-conservation equation

$$\frac{\partial S}{\partial t} = -w\frac{\partial S_{br}}{\partial z}, \tag{5.4}$$

while the thermal energy equation 1.9 is integrated in the modified form

$$c\frac{\partial T}{\partial t} + c_w w\frac{\partial T}{\partial z} = \nabla \cdot (k\nabla T), \tag{5.5}$$

where $c_w = \rho_{br}c_{br} + \rho_s L/[T_m - T(z)]$.

It is important to note that all three models are approximate, and the question is rather whether they are reasonable and convenient parameterisations of brine drainage, having the correct phenomenology. The models of Turner *et al.* and of Rees Jones & Worster are faithful to the physics that convection is a global process (communicated through the pressure field) rather than a sum of local processes. The models of Griewank & Notz and of Rees Jones & Worster are faithful to the physics that $w(z_c) = 0$ when $z_c = 0$, whereas the model of Turner *et al.* gives a non-zero vertical velocity at the ice surface when there is whole-layer convection. On the other hand, the models of Griewank & Notz and of Turner *et al.* have the property that $w$ is continuous in time, which may make for easier, less costly calculation, whereas $w$ can jump discontinuously in

the model of Rees Jones & Worster, which is an inconvenience that potentially reduces the order of convergence of numerical schemes implementing the model, though it may reflect the physics of brine channels switching on and off as conditions affecting the Rayleigh number vary.

All three models capture important dynamics. They can all predict the sort of delay in the onset of brine drainage seen in some experiments [10], [21]. This may not be an important delay in natural settings given that the early stages of ice growth in open ocean can involve accumulations of frazil into grease ice or pancake ice, for example, before the consolidated regime begins. On the other hand, the physics causing such a delay, that the Rayleigh number is insufficiently large, can occur in later stages of ice growth as the atmospheric and oceanic heat fluxes vary. Related to that, they can all predict enhancement or re-initiation of brine drainage during periods of warming [20]. And they all adjust their dynamics to different oceanic salinities and should work as well in the Baltic, for example, as in the central Arctic.

A representative calculation of growth is shown in figure 6. For the calculation shown, the ocean has salinity 35 ppt and temperature $-2^\circ$C. The heat flux from the ocean is calculated from a $\frac{4}{3}$-power-law convective parameterisation to be approximately 6 W m$^{-2}$. The surface heat flux to the atmosphere and surface temperature are related simply using a heat-transfer coefficient of 20 W m$^{-2}$ $^\circ$C$^{-1}$, with a fixed atmospheric temperature of $-20^\circ$C. The vertical velocity was calculated using equation 5.3 with $\alpha = 0.003$ and $R_c = 5$. We see that, in this monotonic-growth scenario, the temperature field remains approximately linear, the salinity decreases over the 100 days simulated to a modal value of about 6 ppt, while the brine volume also decreases to a modal value of less than about 0.1. In consequence of the ever-changing porosity, the maximum Rayleigh number is maintained at a roughly constant size. Many other scenarios have been explored, particularly by Griewank & Notz [20].

The brine flux predicted by this model is shown as a function of time in figure 1. In comparison, the dashed curve shows the prediction of a zero-layer Semtner model with the same boundary conditions, with brine fluxes determined by assuming a fixed ice salinity of 4 ppt. The very close agreement between these two models at late times is coincidental and unexpected given the approximate nature of the examples chosen here for illustration and the fact that the two calculations give rather different predictions (not shown) of the thickness of sea ice as a function of time. However, the correspondence of the functional forms predicted is relevant and indicates that the convective model can be tuned to give similar long-term trends as a fixed-salinity model for a given scenario.
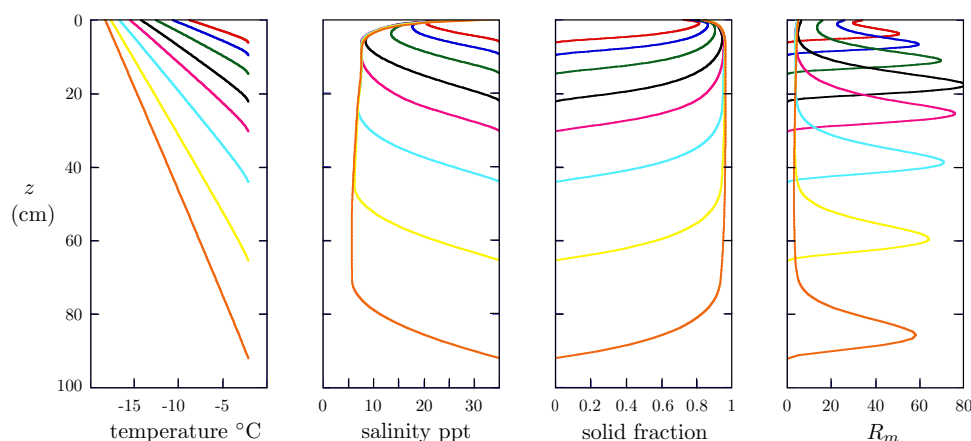


**Figure 6.** Vertical profiles of temperature, salinity, solid fraction and Rayleigh number $R_m$ as they evolve in time according to the one-dimensional model described above [21]. From the top downwards the profiles are at times of 0.5, 1, 2, 4, 7 14, 30, 60 days after the start of ice formation.

# 6. Discussion and Conclusions

Brine drainage from sea ice is a complex process involving interactions between fluid flow in a porous medium and phase change that affects the fluid-mechanical properties of the medium. All of that happens on horizontal scales of millimetres to centimetres, and the internal flows are intrinsically three-dimensional on those scales. An understanding of the underlying physics has led to the recent emergence of one-dimensional models that seem capable of predicting the evolution of mean vertical salinity profiles in sea ice. While enormously more simple and cost-effective than two-dimensional or three-dimensional models of the resolution required to capture brine channels, these schemes do increase the computational cost relative to current operational ice components of climate models, so questions arise whether they are feasible given current resources and whether they are worthwhile.

Preliminary calculations [19] suggest that equations 5.4 and 5.5 can be evaluated effectively using as few as four layers in the vertical, with results in reasonable agreement with calculations made using 100 layers in the vertical and with field data [14].

The long-term trends of salt flux versus growth rate evaluated using climatological data to determine ocean and atmospheric heat fluxes [20] suggest that, when averaged over a week, a linear relationship between salt flux and growth rate, as used in current models, gives a good approximation, so the sophistication and cost of evaluating the salinity of sea ice dynamically may not be worthwhile. On the other hand, such a coarse-grained view averages over periods of rapid growth while the ice is thin and periods of rapid drainage during warming events. Such periods may be very important dynamically, particularly perhaps during the early formation of sea ice in leads, for which buoyancy fluxes are localised spatially as well as temporally. Like clouds with respect to heat fluxes in the atmosphere, such localised convective events may create significant counter-gradient salt fluxes, which would need to be taken into account for a proper understanding and quantification of oceanic forcing.

So, while simple segregation models may be sufficient to determine thermal properties of sea ice, the development of convective schemes along the lines presented above seems worthwhile, to give better representations of buoyancy fluxes as they vary in time, to be robust in the face of regional variations of ocean salinity or scenarios of ocean freshening, and to provide estimates of the velocity fields inside sea ice that can transport biogeochemical materials such as nutrients for marine life.

## Acknowledgment

## References

1. Feltham, D.L., Untersteiner, N., Wettlaufer, J.S. & Worster, M.G. 2006 Sea ice is a mushy layer. *J. Geophys. Res.* **33(14)**, L14501.
2. Semtner, Jr., A.J. 1976 A model for the thermodynamic model of sea ice in numerical investigations of climate. *J. Phys. Oceanogr.* **6**, 379?389.
3. Maykut, G.A. & Untersteiner, N. 1969 Numerical prediction of the thermodynamic response of Arctic sea ice to environmental changes. *The Rand Corporation, Santa Monica, Calif.* RM-6093-PR
4. Worster, M.G. 1992 The dynamics of mushy layers. In *Interactive Dynamics of Convection and Solidification*. NATO ASI Series **E219**, 113–138. Kluwer.
5. Hunke, E.C. & Lipscomb, W.H. 2008 The Los Alamos sea ice model user's manual, version 4. *Tech. Rep. LA-CC-06-012* Los Alamos Natl. Lab., Los Alamos, NM.
6. Vancoppenolle, M, Goosse, H., De Montety, A., Fichefet, T., Tremblay, B. & Tison, J-L. 2010 Modeling brine and nutrient dynamics in Antarctic sea ice: The case of dissolved silica. *J. Geophys. Res. Oceans* 115, C02005.
7. Huppert, H.E. & Worster, M.G. 2012 Flows involving phase change. In *Environmental Fluid Dynamics Handbook.* Edited by H.J. Fernando. CRC Press.

8. Chung, C.A. & Worster, M.G. 2002 Steady-state chimneys in a mushy layer. *J. Fluid Mech.* **455**, 387–411.

9. Worster, M.G. 1992 Instabilities of the liquid and mushy regions during solidification of alloys. *J. Fluid Mech.* **237**, 649–669.

10. Wettlaufer, J.S., Worster, M.G. & Huppert, H.E. 1997 Natural convection during solidification of an alloy from above with application to the evolution of sea ice.*J. Fluid Mech.* **344**, 291–316.

11. Worster, M.G. 2000 Solidification of fluids. In *Perspectives in Fluid Dynamics – a Collective Introduction to Current Research.* Edited by G.K. Batchelor, H.K. Moffatt and M.G. Worster. pp. 393–446. CUP.

12. Aussillous, P., Sederman, A.J., Gladden, L.F., Huppert, H.E. & Worster, M.G. 2006 Magnetic Resonance Imaging of structure and convection in solidifying mushy layers. *J. Fluid Mech.* **552**, 99–125.

13. Peppin, S.S.L., Huppert, H.E. & Worster, M.G. 2008 Steady-state solidification of aqueous ammonium chloride. *J. Fluid Mech.* **599**, 465–476.

14. Notz, D. & Worster, M.G. 2008 In-situ measurements of the evolution of young sea ice. *J. Geophys. Res.* **113**, C03001.

15. Freitag, J. 1999 Hydraulic properties of Arctic sea ice: Implications for the small scale particle transport. *Rep. Polar Res.*, **325**, 1–150.

16. Wells, A.J., Wettlaufer, J.S. & Orszag, S.A. 2013 Nonlinear mushy-layer convection with chimneys: Stability and optimal solute fluxes. *J. Fluid Mech.* **716**, 203–227.

17. Wells, A.J., Wettlaufer, J.S. & Orszag, S.A. 2011 Brine fluxes from growing sea ice. *Geophys. Res. Lett.*. **38**, L04501.

18. Rees Jones, D.W. & Worster, M.G. 2013 Fluxes through steady chimneys in a mushy layer during binary alloy solidification. *J. Fluid Mech.* **714**, 127–151.

19. Turner, A.K., Hunke, E.C. & Bitz, C.M. 2013 Two modes of sea-ice gravity drainage: A parameterization for large-scale modelling. *J. Geophys. Res. Oceans* **118**, 2279–2294.

20. Griewank, P.J. & Notz, D. 2013 Insights into brine dynamics and sea ice desalination from a 1-D model study of gravity drainage. *J. Geophys. Res. Oceans* **118**, 3370–3386.

21. Rees Jones, D.W. & Worster, M.G. 2014 A physically based parameterisation of gravity drainage for sea-ice modelling. *J. Geophys. Res. Oceans* **119**, doi:10.1002/2013JC009296.

22. Hunke, E. C., Lipscomb,W. H. Turner, A. K. Jeffery, N. & Elliott, S. 2013 CICE: The Los Alamos sea ice model documentation and software user's manual, version 5.0, *Tech. Rep. LA-CC-06-012*, Los Alamos Natl. Lab., Los Alamos, N. M.